# DEVELOPMENT AND EVALUATION OF A CONTINUOUS FLOW BIOCHAR UNIT USING RICE HUSK BIOMASS

/

تطوير وتقييم وحدة الفحم الحيوي ذات التدفق المستمر للكتلة الحيوية لقشور الأرز

**Hesham A. FARAG, Mohamed M. EL-KHOLY, Mahmoud OKASHA*, Ahmed E. AZAB, Ahmed E. KHATER, Reham M. KAMEL**

Agricultural Engineering Research Institute (AEnRI), Agricultural Research Center (ARC), Giza 12611/ Egypt

*Tel: +20-1003133841; E-mail: mahmoudokasha1988@yahoo.com*

*Corresponding author: Mahmoud Okasha*

*DOI: https://doi.org/10.35633/inmateh-72-03*

***Keywords:*** *Rice husk; Biochar; Pyrolysis; Continuous flow*

## ABSTRACT

*This study aims to develop and evaluate a locally manufactured carbonization unit with a screw conveyor. Various carbonization temperatures (350, 400, and 450°C) and feeding rates (50, 75, and 100 kg/h) were examined to determine optimal conditions for producing biochar from rice husk (RH). The results revealed that increasing the pyrolysis temperature from 350 to 450°C decreased RH biochar yield, while increasing the feeding rate from 50 to 100 kg/h increased it. Ash content was 22.4% at 350°C for 100 kg/h, and the maximum value was 31.4% at 450°C and 50 kg/h. The BET surface area of the biochar increased from 105.71 to 312.32 $m^2$/g at 450°C, with slight non-significant changes at a 100 kg/h feed rate. RH biochar showed decreasing H and O values with higher temperatures and lower feed rates. RH biochar at 450°C and 50 kg/h showed increased macro porosity and surface area, rendering it suitable for agricultural application as a soil amendment.*

**الملخص**

تهدف هذه الدراسة إلى تطوير وتقييم وحدة انحلال حراري مستمر من النوع اللولبي محلي الصنع. تم تقييم الوحدة عند درجات تحلل حراري مختلفة (350، 400 و450 درجة مئوية) ومعدلات تغذية (50، 75 و100 كجم/ساعة) لتحديد الظروف المثالية لإنتاج الفحم الحيوي من قشر الأرز. وأظهرت النتائج أن بزيادة درجة التحلل الحراري من 350 إلى 450 درجة مئوية أدت الى انخفاض إنتاجية الفحم الحيوي الناتج من قشر الأرز، بينما بزيادة معدل التغذية من 50 إلى 100 كجم/ساعة أدت الى زيادة إنتاجية الفحم الحيوي. بلغ محتوى الرماد 22.4٪ عند درجة تحلل حراري 350 درجة مئوية ومعدل تغذية 100 كجم/ساعة، وكانت القيمة القصوى 31.4٪ عند 450 درجة مئوية و50 كجم/ساعة. زادت قيمة مساحة سطح *BET* للفحم الحيوي الناتج من 105.71 إلى 312.32 م$^2$/جم عند 450 درجة مئوية، مع تغييرات طفيفة وغير معنوية عند معدل تغذية 100 كجم/ساعة. أظهر الفحم الحيوي الناتج من قشر الأرز انخفاضًا في قيم الهيدروجين والاكسجين مع درجات الحرارة المرتفعة ومعدلات التغذية المنخفضة. أظهر الفحم الحيوي الناتج من قشر الأرز عند درجة تحلل حراري 450 درجة مئوية ومعدل تغذية 50 كجم/ساعة زيادة في المسامية الكلية ومساحة السطح، مما يجعله مناسبًا للتطبيق الزراعي كمحسن للتربة.

## INTRODUCTION

Annually, large amounts of biomass by-products are produced as a result of human activities. Agriculture ranks as one of the most common human activities that produce large amounts of biomass, and the incorrect treatments for these by-products make it harmful to the environment and help to increase the destructive impacts of climate change. The climate change phenomenon is undeniably one of the utmost pressing concerns globally. Global warming is a consequence of the mounting levels of carbon dioxide and different greenhouse gases in the atmosphere. The climate crisis likely will require a large quantity of CO2 to be removed from the atmosphere. Biochar production for agricultural use has a good potential for solving the global warming problem. Its storage in soils has been suggested to decrease climate change by sequestering carbon inside the soil. It has a long period of stability, lasting hundreds to thousands of years (*Sun et al., 2020; Ren et al., 2022*).

Biochar is a carbon-rich black solid, mainly generated from biomass through pyrolysis processes; pyrolysis allows producing biochar by heating in the lack of oxygen. Besides the biochar, the pyrolysis processes also give other products like bio-oils and synthesis gas or syngas that could be further used as renewable fuels (*Sun et al., 2020*). Moreover, biochar has attained extensive interest globally owing to its verified capacity to enhance soil health (*Ren et al., 2023*), soil fertility (*Ding et al., 2016*), and increased water-holding capacity as an inexpensive sorbent (*Qu et al., 2021*). Due to these reasons, developing pyrolysis technologies for biochar production continues to be an urgent task on a global scale. The word pyrolysis has two Ancient Greek Words; the first is Pyro, which means fire, and the second is Lysis, which means separating (*Ibrahim, 2020*). Pyrolysis is the thermal degradation of biomass that occurs due to a lack of oxygen at

temperatures varying from 300 to 800°C. In a three-stage reaction, pyrolysis necessitates using kilns and furnaces to heat the biomass. At the first manufacturing stage, the biomass loses water and other wastes. The residue is then pyrolyzed again, and biochar is formed. Ultimately, the biochar decomposes to generate the carbon-rich charcoal employed in applications (*Demirbas, 2004*). The pyrolysis process can be categorized as slow, quick, rapid, and flush. Although there are no significant differences between these alternatives and their derivatives, slow pyrolysis is the proper method for producing the target biochar (*Demirbas et al., 2006*).

Rice husk (RH) is one of the most used raw materials in producing biochar. Moreover, RH is a plentiful by-product in rice-producing countries. Around 822 million tons of rice husks are produced globally; however, they are underutilized because of the limited recycling options (*Dunnigan et al., 2018*). Rice plays a pivotal role in agricultural sector of Egypt. In 2019, over 503,000 hectares of rice were planted. This area produced about 0.9 million tons of rice husk. This important rice by-product should be considered a sustainable national source instead of being left or burned, causing terrible environmental and health hazards. Conversion of RH to biochar has good potential and benefits for sustainable waste recycling, energy production, carbon sequestration, soil quality enhancement, and improved plant growth (*Abrishamkesh et al., 2015*).

Biochar can be used as a soil conditioner, improving plant growth by providing and keeping nutrients and offering further services, including enhancing biological and physical properties of the soil (*Lehmann and Rondon, 2006*). Biochar has a higher porosity and surface area than other soil organic matter (SOM) types. It can enhance soil structure and water retention by improving soil aggregation and texture (*McElligott et al., 2011*). Biochar also affects the soil bulk density, which might decrease by adding biochar, particularly at high application rates, because of its relatively lower bulk density than mineral particles (*Lehmann and Joseph, 2015*). The organic carbon of the biochar improves soil aggregation and aggregate stability. Furthermore, changes in soil structure enhance soil water retention and infiltration, resulting in less runoff and erosion (*Gwenzi et al., 2015*). Some soil characteristics, on the other hand, may improve over time rather than immediately after treatment (*Mukherjee and Lal, 2014*).

Biochar-producing systems are categorized as gasifiers or pyrolizers and, depending on the technology utilized, create three distinct products: biochar, syngas, and bio-oil (*Scholz et al., 2014*). Currently, waste and biomass management by the thermo-pyrolysis process to produce high-value products requires the improvement of more selective, controlled, multi-product, and integrated pyrolysis units. Pyrolysis furnaces should be designed and manufactured with a perfect model in mind; Even if a usual formula has produced relevant results in other contexts, it should be applied carefully. *El-Sheikha and Hegazy* (*2020*) designed and assessed a biochar pyrolysis kiln to produce biochar from two agricultural residues (i.e., rice straw and date palm fronds). Their results revealed the possibility of utilizing agricultural residues to produce biochar. In the same trend, a double-chamber down draft (DcDD) pyrolizer was constructed and tested using rice husk to produce biochar. Its results indicated that the DcDD reactor is an appropriate choice for turning waste biomass into biochar that improves the soil characteristics in agricultural settings (*Alahakoon et al., 2022*).

Therefore, this study aims to use rice husk as a biomass feedstock to produce superior-quality biochar using a continuous screw-type pyrolysis furnace that features easy operation and maintenance.

## MATERIALS AND METHODS

### *Description of biochar-producing system*

The biochar-producing system consists of the following main units (i.e., feeding unit, carbonization unit with horizontal screw conveyor, biochar outlet unit, filtration and condensing units, and the control unit), as shown in Fig.1.

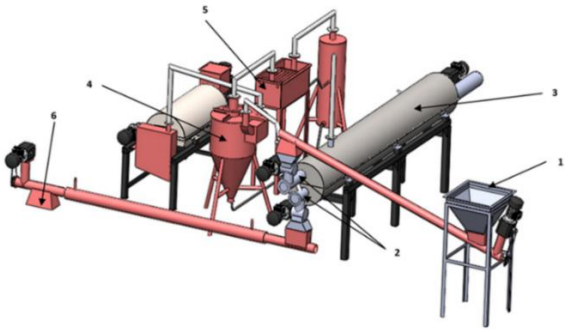


**Fig. 1 – 3D view of the continuous screw model of the biochar system**

*1 – Feeding unit; 2 – Horizontal screw conveyor; 3 – Carbonization unit chassis; 4 – Cyclone; 5 – Condenser unit; 6 – Biochar outlet unit*

***The feeding unit***

The feeding unit comprises a raw material feeding hopper and an inclined raw feeding screw. A square-shaped raw material hopper made of an iron sheet with a thickness of 3 mm, dimensions of 80 × 80 × 65 cm, and a slope angle of 60° on all sides was used to feed the system with rice husk. The feeding hopper is fixed within four supporting legs with a length of 173 cm. The inclined feeding screw has a 12.5° inclination angle, a 450 cm length, a 15.2 cm diameter, and a 10.1 cm screw pitch, enclosed in a tubular housing with a 16.0 cm diameter. A 1.5 kW three-phase electric motor powered the inclined feeding screw with a reduction gearbox to elevate the RH from the feeding hopper to the screw conveyor in the carbonization unit. A 0.55 kW three-phase motor feeds RH to the carbonization unit.

***Horizontal screw conveyor and carbonization unit***

The horizontal screw conveyor conveys the rice husk (raw material) into the carbonization unit. A horizontal screw with a two-ways carbonization cylinder was chosen to reduce the total length of the carbonization unit. The horizontal screw with a two-way (forward and backward) carbonization cylinder has the same diameter and pitch of 15.2 cm. The length of the forward screw is 520 cm, whereas the backward screw measures 475 cm in length, and each screw is powered by a three-phase electric motor with a power of 2.2 kW. The two-way screws are placed in a tubular housing with a diameter of 16 cm. The carbonization unit consists of a heating stove and carbonization cylinders. The heating stove is the outer body of the carbonization chamber and consists of a double-layer cylinder. A thermal insulator was placed between the double cylinder for energy-saving purposes. The carbonization chamber is the essential part of the carbonization unit, where the thermo-pyrolysis process occurs, and the other parts are linked to this part. The inner cylinder (pyrolysis chamber) is made of steel with a thickness of 10 mm and an internal diameter of 15.24 cm. It is also airtight to withstand temperatures above 800°C and achieve low oxygen levels during pyrolysis. The carbonization tank length is 535 cm, and the diameter is 75 cm. Two K-type thermocouples were located along the horizontal axis of the outer cylinder. The thermocouples with an accuracy of ±2.5°C and a temperature range of 0–1600°C with a probe diameter of 13 mm and length of 35 cm were used to measure the internal chamber temperature. The carbonization unit was heated through a flame hole placed at the beginning of the unit with an internal diameter of 15 cm. During operation, the exhaust gases exit through a smokestack on the top of the carbonization tank.

***Carbonization unit chassis***

The carbonization unit chassis is made of square hollow steel sections shaped (10 × 10 cm) with a thickness of 3 mm and overall dimensions of 400 × 97.5 × 135 cm (L × W × H), respectively. It was used to carry the carbonization unit and the screw conveyor. In addition, the chassis has six subsidizing legs in a square hollow section (10 × 10 cm) with a thickness of 3 mm to attain the required operating height.

***The filtration and condensing units***

Developed biochar system generated steam, fumes, and dust. It has a cyclone, condenser, dry scrubber, and steel connecting tubes. The ignition sources in this system are feedstock or syngas. The fume treatment unit processes the smoke, where it is separated into distinct elements; coal tar is discharged from the cyclone, while bio-oil emerges from the dry scrubber. A condensing unit comprises a condenser (heat exchanger) and a suction fan. The condenser, which had a water cooler, was used to cool the gas and generate liquid distillate compounds (bio-oil) through condensation. A 13.2 V DC motor-driven suction fan was employed to draw the generated syngas and additional vapors from the syngas tank, pushing them through the firing system to decrease fuel consumption. The condenser of the filtration unit concentrates the vapor to produce the bio-oil, and the other gas mix is directed to the filter groups to produce syngas, which is stored in the syngas tank and used in the firing system to reduce fuel consumption. For the last stage, a dry scrubber comprises a cylinder of 50 cm in diameter and 1.5 m in height. It was used to separate the steam from the condenser to produce syngas to reuse for ignition, provide the energy needed to heat the reactor and obtain bio-oil.

***The biochar outlet unit***

This unit comprises a horizontal screw with a length of 450 cm; it has the same diameter and pitch of 15.2 cm and is operated by a three-phase motor with a power of 1.1 kW. The horizontal screw of biochar is placed in a tubular housing with a diameter of 16.0 cm, and at the end of this screw, a biochar outlet is assembled.

***The control unit***

The control unit has switches to turn on and off the motors, an inverter (model: ATV71HU22N4Z Schneider Electric, Taiwan) to control and change the speeds of the feeding motors, an indicator linked to the temperature sensors to display the temperature inside the reactor, and a voltmeter indicator to display the voltage and amperage while the motors are running.

***Raw materials***

Rice husk was utilized as a raw material to yield biochar using the developed screw continues model reactor. The rice husk was obtained from local medium-scale mills in Kafr El-Sheikh, Egypt. Before being used in the trials, the obtained rice husks were air-dried and stored. The proximate and elemental RH analyses were determined using the Perkin Elmer Thermo gravimetric analyzer and EA 1112 elemental analyzer, and the results are recorded in Table 1.

**Table 1**

**Elemental and proximate analysis of rice husk (raw material)**

| **Elemental analysis** | **Value** |
|---|---|
| Carbon (wt%) | 40.89 ± 4.25 |
| Hydrogen (wt%) | 3.56 ± 0.48 |
| Nitrogen (wt%) | 4.73 ± 0.26 |
| Oxygen (wt%) | 53.72 ± 6.30 |
| **Proximate analysis** | **Value** |
| Bulk density (kg/cm$^3$) | 120 ± 11.65 |
| Moisture (%) | 11.9 ± 0.38 |
| Ash (dry) (%) | 8.67 ± 1.25 |
| Fixed carbon (%) | 15.68 ± 1.06 |
| Volatile compounds (%) | 74.52 ± 5.94 |

* The data was expressed using the mean ± standard deviation (SD).

***Experimental site***

The biochar system was constructed and evaluated by the Agricultural Engineering Research Institute in cooperation with the Academy of Scientific Research and Technology. The Experimental investigations were executed in Egypt at the Rice Mechanization Center, Kafr El-Sheikh Governorate, at coordinates 31°06′58.67″ N latitude and 30°51′17.53″ E longitude.

***Methods***

First, the ignition of the carbonization unit was achieved by utilizing a Liquefied Petroleum Gas (LPG) cylinder. (43.1 MJ/kg calorific value) for 100% energy supply; when the unit reached 250-450°C, syngas shared about 50% of the energy needed for the carbonization process, saving about 50% of energy cost. According to the previous references, biochar is produced at temperatures between 250-450°C, depending on the source of residues and the quality needed. Rice husk residual (Sakha 101 cv., *Oryza sativa* L.) was carbonized under different degrees of carbonization temperature (350, 400, and 450°C) plus feeding rates of 50, 75, and 100 kg/h to optimize the production of biochar from RH. Each temperature or residence time has been controlled using the electrical control panel. Before feeding the RH (raw material) to start the pyrolysis process, the reactor should be at the desired temperature for executing the trials. The energy supply from the heat source should be greater during startup than at a steady state. Thus, the system takes approximately 2 hours at the beginning of the process to reach the pyrolysis temperature, relying on radial temperature gradient of the pyrolysis chamber. The indirect heating system of this study dilutes syngas less than direct heating. Consequently, concentrated syngas could produce biochar for combustion zone energy (*Joardder et al., 2017*).

***Scanning electron microscopy (SEM) and Fourier transform infrared spectroscopy (FTIR) analysis***

Scanning electron microscopy (SEM, Hitachi, S-570) was used according to *Liu et al.* (*2015*) to evaluate the biochar samples' morphological alterations with a high vacuum at a 20 kV accelerating voltage and a 6000x magnification magnitude. Fourier transform infrared spectroscopy (FTIR) was also assigned between 600 and 4000 cm$^{-1}$ utilizing the method of attenuated total reflectance (ATR). Moreover, 0.5 mg of each sample was put into the Ge window of Nicolet FTIR instrument, equipped with an ATR attachment, after being ground to a 0.1 mm particle size. A KBr beam sampler was used to analyze the samples' spectra, conducting over 256 scans. The FTIR data was acquired with 4 cm$^{-1}$ resolution and 32 scans using a diamond ATR attachment.

***Biochar yield and physical properties***

The determination of biochar yield was performed following the procedure described by *Lynch and Joseph* (*2010*), as shown in Eq. 1:

$$Biochar\ yield\ (\%) = \frac{M_1}{M_2} \times 100 \quad (1)$$

where: $M_1$ stands for the mass of the biochar [g], and $M_2$ stands for the mass of air-dried raw materials [g].

The ash content was calculated using the dry combustion technique. Briefly, 5.0 g of biochar was heated to 500°C for 8 h. Once the crucible had reached the ambient temperature, it underwent re-weighing (*Song and Guo, 2012*). Finally, the ash percentage was determined using Eq. 2:

$$Ash\ content\ (\%) = \frac{M_{Ash}}{M_1} \times 100 \quad (2)$$

where $M_{Ash}$ is the ash mass [g].

The specific surface area and total pore volume of the biochar can be determined using the Brunauer-Emmett-Teller method and an Autosorb-1 surface area analyzer (Quantochrome Instruments, USA).

***Elemental analysis***

The carbon (C), oxygen (O), hydrogen (H), and nitrogen (N) content of the biochar was calculated utilizing an X-ray fluorescence spectrometer (XRF) manufactured by Malvern Panalytical Almelo in the Netherlands (CNHOS). The Bray II technique determined the amount of (P) *(Bray and Kurtz, 1945*). The approach outlined by *Samsuri et al.* (*2014*) was employed to analyze the tradable elements, such as magnesium (Mg), potassium (K), silicon (Si), and aluminum (Al).

***PH, electric conductivity (EC), and cation exchange capacity (CEC)***

The method developed by *Savova et al.* (*2001*) was utilized to determine the pH of biochar. In a 100mL conical flask, 4.0 g of biochar was dissolved in water. The flask was prepared by filling it with boiling water, which was subsequently covered with a watch glass and allowed to cool. The supernatant was then drained. The supernatant was allowed to cool to ambient temperature before pH was measured by a Metrohm 827 pH Lab (USA). The EC of the biochar was measured utilizing the CON 700 EC meter (Eutech Instruments, USA) after wetting it with deionized water at a solid-to-water ratio of 1:5 and agitating the mixture for 24 h.

*Song and Guo* (*2012*) method was used to measure the cation exchange capacity (CEC). In a 50-mL Falcon tube, about 0.50 g of biochar was mixed with 40 mL of 1 M ammonium acetate. Then, the mixture was carefully stirred for a complete 24-hour timeframe. A vacuum pump was used to filter the mixture, and after that, 40 mL of ammonium acetate was added. Then, 30 mL of isopropanol was decanted into the vacuum pump in three equal portions. 50-mL dosages of 1 M KCl were used to leach the remaining biochar, and the leachate was collected. An auto-analyzer (QuikChem 8000 Series FIA+ System; Lachat Instruments, USA) was utilized to quantify the extracted NH4+ content, while atomic absorption spectrometry (AAnalyst 400; PerkinElmer, USA) was employed to assess exchangeable cations of the biochar.

***Statistical analysis***

An SPSS 26.0 program (IBM Corporation, USA) was used to analyze the data. For multiple comparisons, two-way analysis of variance (ANOVA) and post hoc (Tukey test) were employed. Differences were considered statistically significant at a level of 0.05.

## RESULTS AND DISCUSSION

***SEM and FTIR analysis***

Figure 2 illustrates the cellular microstructure of the biochar (shown by SEM microscopy), which consists of numerous hollow channels of varying diameters formed from tracheid cells. The SEM micrographs displayed the porous structures of the resultant biochar, revealing different sizes and shapes of the micropores, and mesopores. The biochar produced at a temperature of 350°C retained unaltered tissue, leading to incomplete pore formation. Nevertheless, when exposed to a temperature of 450°C, the morphology of the biochar underwent a transformation resembling a honeycomb structure, wherein larger holes interconnected cylindrical holes. Biochar featuring well-structured pore arrangements shows a considerable BET surface area and adsorptive capacity, as indicated by *Guo and Lua* (*1998*). Once the biochar was heated at 450°C, noticeable surface cracks and shrinkage became apparent across different feeding rates. Excessively porous, hollow, spherical particles and well-structured pyrolyzed biochar at 450°C are seen in Fig. 2 [c, f, and i]. The thin walls of the buildings gave them a fragile appearance. The structure of biochar displayed increased organization with an elevation in pyrolysis temperature and with a decrease in the number of micropores and a higher number of large pores. This result is similar to *Claoston et al.* (*2014*).

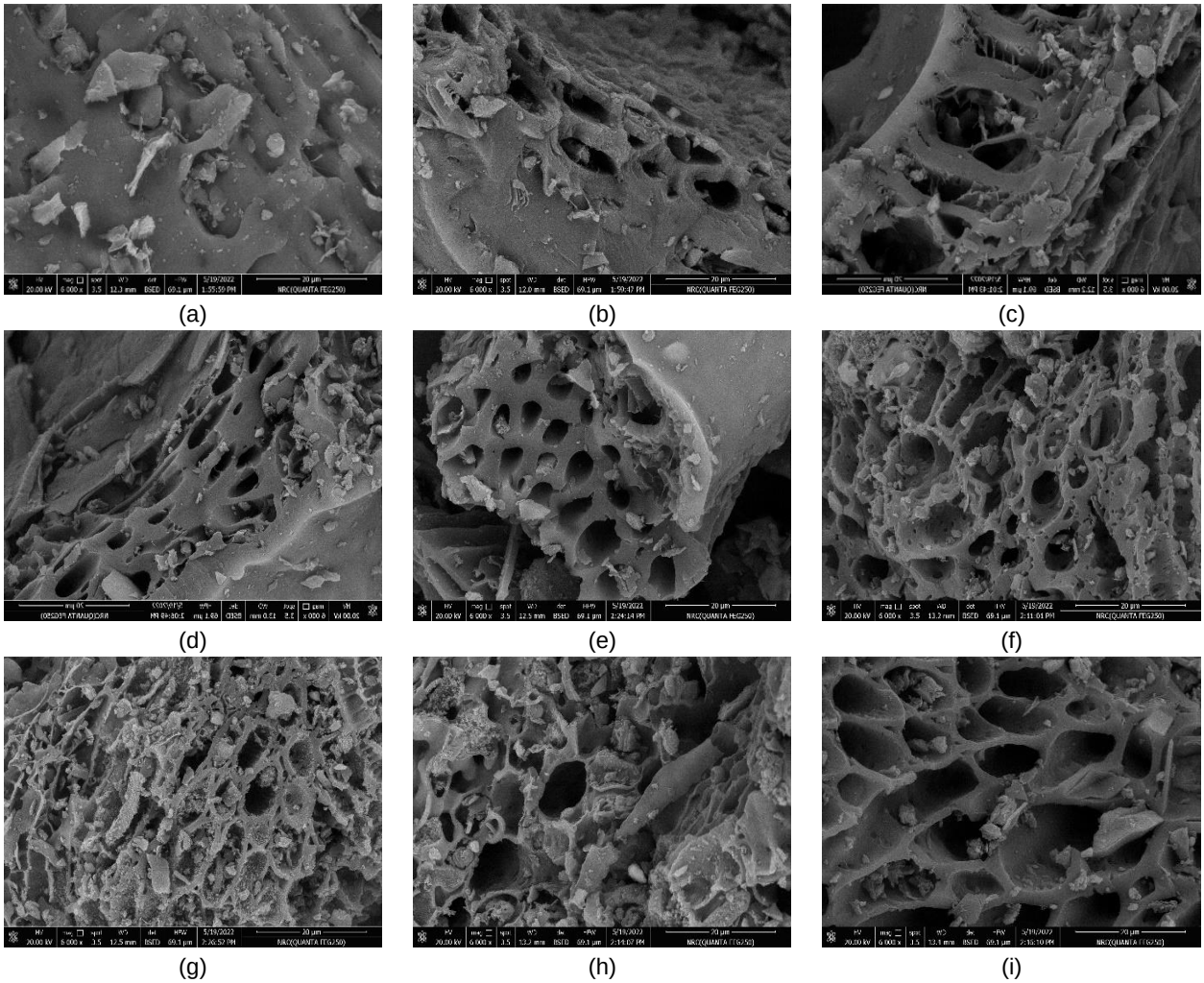

**Fig. 2 – SEM images as a function of the pyrolysis temperatures of 350°C (a, b, and c), 400°C (d, e, and f), and 450°C (g, h, and i) for feeding rates of 50, 75, and 100 kg/h from left to right for every row, respectively**

Fourier transforms infrared (FTIR) spectra of biochar prepared from RH as a function of wavenumber at different pyrolysis temperatures are presented in Fig. 3. Table 2 shows the specific chemical bonding and transmittance observed by FTIR. The change in biochar surface functional groups as a heating function was studied with (FTIR) spectroscopy. The chemical response of the surface also controls adsorption behavior, specifically chemically adsorbed oxygen in different forms of functional groups, in addition to porosity. FTIR was effectively used to investigate the impact of temperature on biochar, but due to the absence of discernible variation in intensity under varied feeding rates, the results from this experiment were omitted.

Table 2 details chemical bonding, peak position, and transmittance. Most FTIR provides characteristics from organic functional groups for analyzing the organic components of the biochar. The peak detected at 3505.35 $cm^{-1}$ is presumably a result of the stretching of organic O-H bonds, potentially arising from water within the sample or minerals possessing hydroxyl groups. An increase in temperature from 350°C to 450°C reduces the intensity of the hydroxyl peak, indicating the degradation of hydroxyl groups and the subsequent release of hydrogen and oxygen atoms. C=C asymmetric stretching occurs at 1579.43 $cm^{-1}$, indicated as a G band in (*Keiluweit et al., 2010*), due to the sp2-hybridization bonding of carbon atoms in the aromatic group of lignin. With the increase in temperature from 350°C to 450°C, the intensity of C-H bending dropped, leading to the gaseous product CH4 in the same trend (*Armynah et al., 2018*). Because of the sp3-hybridization bonding of carbon atoms, the transmittance at 1087 $cm^{-1}$ occurred (*Keiluweit et al., 2010; Armynah et al., 2018*), but the range of 1060.71–1079.99 $cm^{-1}$ was achieved as symmetric C-O stretching for lignin, cellulose, and hemicellulose. The presence of aromatic with C-C stretching is suggested by the transmission peak of 1451.92 $cm^{-1}$ (ester and phenol) (*Claoston et al., 2014*). Nonetheless, a C-H bending peak was detected at 792 $cm^{-1}$, indicating the existence of alkynes. Gases CO2 and CH4 are created when the husk is heated, and the FTIR confirms that these gases correspond to the peaks attributed to the cellulose, hemicellulose, and lignin content of the biomass (*Ma et al., 2015*).

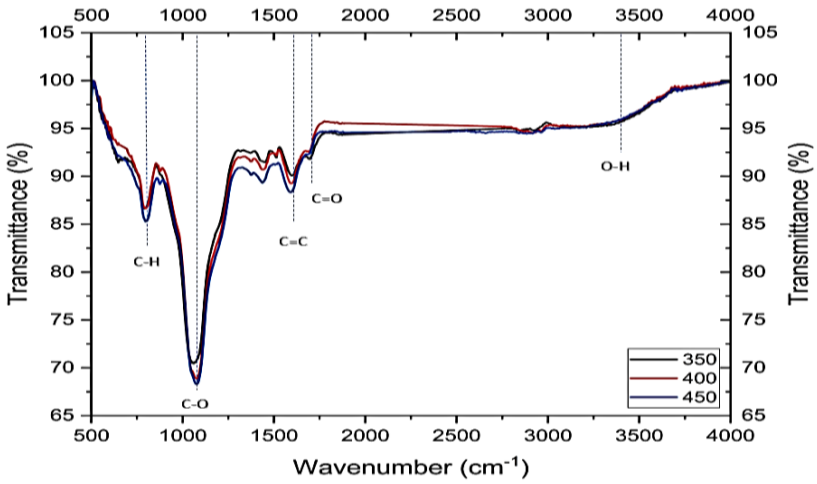


**Fig. 3 – FTIR spectra of rice husk biochar as a function of wavenumber at different pyrolysis temperatures**

**Table 2**

**Peak position and intensity of chemical bonds of RH as a function of pyrolysis temperature utilizing Fourier transform infrared (FTIR)**

| Chemical bond | Peak position and intensity | | |
|---|---|---|---|
| | **350°C** | **400°C** | **450°C** |
| O-H stretching (Lignin, Hemicellulose, Cellulose) | 3509.93 $cm^{-1}$ | 3506.54 $cm^{-1}$ | 3505.35 $cm^{-1}$ |
| | 96.82 | 96.57 | 96.93 |
| C=O Stretching (Lignin) | Peak no observed | Peak no observed | Peak no observed |
| | - | - | - |
| C=C Asymmetric Stretching (Lignin) | 1579.43 $cm^{-1}$ | 1592.09 $cm^{-1}$ | 1590.73 $cm^{-1}$ |
| | 90.71 | 89.26 | 88.43 |
| C-O Stretching (Hemicellulose) | Peak no observed | Peak no observed | Peak no observed |
| | - | - | - |
| C-C Stretching (Hemicellulose) | 1451.92 $cm^{-1}$ | 1441.31 $cm^{-1}$ | 1436.64 $cm^{-1}$ |
| | 88.34 | 90.71 | 97.47 |
| C-O Stretching C-OH Bending (Hemicellulose, Cellulose) | 1074.21 $cm^{-1}$ | 1060.71 $cm^{-1}$ | 1079.99 $cm^{-1}$ |
| | 68.32 | 68.86 | 70.46 |
| C-H Bending (Lignin) | 791.09 $cm^{-1}$ | 799.68 $cm^{-1}$ | 797.11 $cm^{-1}$ |
| | 80.33 | 79.74 | 78.50 |

***Elemental analysis***

Table 3 shows the elemental composition of RH biochar. At feeding rates of 50 and 100 kg/h, the carbon content (C) exhibited a range of 63.34% to 79.14% and 693.4% to 77.33%, respectively. The maximum value of 79.14% was achieved at a 50 kg/h feeding rate and a pyrolysis temperature of 450°C. The high carbon content of biochar with higher pyrolysis temperatures suggests that higher pyrolysis temperatures promote carbonation (*Chen et al., 2012; Nan et al., 2021*). This reduction was caused by the high level of polymerization of the biochar, which resulted in a more condensed carbon structure (*Tomczyk et al., 2020*). The increase in carbon may also be a reason for losing oxygen and hydrogen from the biochar as the pyrolysis temperature rises (*Antal and Grønli, 2003*). In opposition, H and O dropped with increasing carbonization temperature, as *Keiluweit et al.* (*2010*) and *Southavong et al.* (*2018*) also demonstrated.

At both the minimum and maximum feeding rates, the total nitrogen content decreased from 1.74 to 1.36% and 1.54 to 1.45%, respectively, as the corresponding pyrolysis temperature increased (Table 3). The reason is that when the plant biomass is pyrolyzed, its nitrogen-containing structures, including amino acids, amino sugars, and amines, are converted into heterocyclic N aromatic structures (*Cao and Harris, 2010*). This means that the nitrogen will be available and will not decompose immediately but will be released with increasing duration of carbonation.

As shown in Table 3, the element components also display P, K, Mg, Al, and Si for the generated biochar from RH. According to X-ray fluorescence spectroscopy (XRF) results, the considerable ash elements in RH biomass are P, K, and Si. At 450°C pyrolysis temperature and 50 kg/h feeding rate, their respective values are 0.54, 1.64, and 42.14 g/kg.

**Table 3**

**Elemental analysis of rice husk biochar for each specific treatment**

| Biochar characteristics | Pyrolysis temperature, °C | 350°C | | | 400°C | | | 450°C | | |
|---|---|---|---|---|---|---|---|---|---|---|
| | Feeding rate, kg/h | 50 | 75 | 100 | 50 | 75 | 100 | 50 | 75 | 100 |
| Elemental analysis | Carbon (%) | 63.34 ± 4.05 c | 62.92 ± 2.99 c | 61.3 ± 3.85 c | 73.73 ± 6.62 b | 73.68 ± 5.36 b | 72.18 ± 6.78 b | 79.14 ± 4.26 a | 78.68 ± 5.01 a | 77.38 ± 2.87 ab |
| | Hydrogen (%) | 4.80 ± 0.21 a | 4.10 ± 0.12 b | 3.81 ± 0.41 c | 1.04 ± 0.35 f | 2.07 ± 0.25 de | 2.25 ± 0.27 d | 1.08 ± 0.13 f | 1.90 ± 0.00 e | 1.00 ± 0.00 f |
| | Oxygen (%) | 20.01 ± 2.36 d | 22.74 ± 4.05 bc | 22.01 ± 3.84 c | 27.58 ± 2.89 ab | 24.03 ± 4.66 b | 24.23 ± 1.56 b | 28.02 ± 2.01 a | 28.70 ± 0.99 a | 21.99 ± 3.68 c |
| | N (%) | 1.74 ± 0.02 a | 1.63 ± 0.04 bc | 1.54 ± 0.03 c | 1.60 ± 0.02 bc | 1.57 ± 0.05 c | 1.66 ± 0.09 b | 1.36 ± 0.10 e | 1.40 ± 0.06 de | 1.45 ± 0.01 d |
| | P, g/kg | 0.38 ± 0.08 c | 0.36 ± 0.02 c | 0.35 ± 0.00 c | 0.45 ± 0.00 b | 0.41 ± 0.02 bc | 0.42 ± 0.01 bc | 0.54 ± 0.02 a | 0.52 ± 0.03 ab | 0.51 ± 0.00 ab |
| | K, g/kg | 0.13 ± 0.01 g | 0.05 ± 0.00 h | 0.31 ± 0.01 f | 0.53 ± 0.05 d | 0.41 ± 0.01 e | 0.30 ± 0.02 f | 1.64 ± 0.07 a | 0.62 ± 0.01 c | 0.77 ± 0.03 b |
| | Mg, g/kg | 0.04 ± 0.00 d | 0.05 ± 0.00 d | 0.05 ± 0.00 d | 0.14 ± 0.01 b | 0.10 ± 0.00 c | 0.07 ± 0.00 cd | 0.23 ± 0.02 a | 0.15 ± 0.00 b | 0.12 ± 0.00 bc |
| | Al, g/kg | 0.41 ± 0.02 e | 2.00 ± 0.03 b | 0.39 ± 0.04 e | 0.25 ± 0.04 f | 0.96 ± 0.00 c | 0.17 ± 0.02 g | 0.47 ± 0.01d | 0.87 ± 0.06 cd | 5.66 ± 0.07 a |
| | Si, g/kg | 35.7 ± 2.86 b | 36.85 ±4.36 b | 37.33 ± 5.34 b | 43.3 ± 4.56 a | 38.55 ± 1.09 ab | 39.61 ± 2.85 ab | 42.14 ± 1.25 a | 42.84 ± 5.27 a | 32.24 ± 4.00 c |

### *Physical properties of the produced biochar*

Table 4 displays the physical properties of the biochar derived from RH. The ash content within the resulting biochar experienced a 33% increase when the temperature was raised from 350°C to 400°C, after which it remained constant at higher temperatures. The ash content increases and stabilizes at 19% for grass charcoal, as stated by *Li et al.* (*2013*).

Biochar yield decreased from 45.8% to 39.1% when the pyrolysis temperature was raised from 350°C to 400°C at the feeding rate of 100 kg/h. Furthermore, elevating the pyrolysis temperature from 400°C to 450°C at a 100 kg/h feeding rate decreased biochar yield from 39.1% to 34.2%. Meanwhile, the biochar production rate decreased from 43.6% to 33.9% and from 37.2% to 30.0% as the temperature increased from 350°C to 450°C, at 75 and 50 kg/h feeding rates, in order, as illustrated in Table 4.

The BET surface areas of the generated biochar increased as the pyrolysis temperature within the examined range of 350–450°C rose, as indicated in Table 4. At a feeding rate of 50 kg/h, the BET surface areas for pyrolysis temperatures of 350, 400, and 450°C were 125.71 $m^2$/g, 210.75 $m^2$/g, and 312.32 $m^2$/g, in order. Similarly, at a 100 kg/h feeding rate, the counterparts' BET surface areas were 105.71 $m^2$/g, 187.91 $m^2$/g, and 283.64 $m^2$/g, in order. The values in question were higher when the pyrolysis temperature reached 450°C, likely due to the intense reactions at this temperature, leading to biochar characterized by mesoporous pores. At high pyrolysis temperatures, a rise in surface area is generally caused by removing volatile material, which increases micropore volume (*Ahmad et al., 2012; Tomczyk et al., 2020*).

**Table 4**

**Physical properties of rice husk biochar yielded at various pyrolysis temperatures and feeding rates**

| Pyrolysis temperature, °C | Feeding rate, kg/h | Physical properties | | |
|---|---|---|---|---|
| | | Biochar yield (%) | Ash content (%) | BET surface area ($m^2$/g) |
| 350 | 50 | 37.2 ± 0.39 bc | 23.2 ± 4.76 d | 125.71 ± 3.52 d |
| | 75 | 43.6 ± 2.65 ab | 23.2 ± 1.85 d | 118.63 ± 0.95 de |
| | 100 | 45.8 ± 1.23 a | 22.4 ± 2.96 d | 105.71 ± 1.26 e |
| 400 | 50 | 33.1 ± 0.58 c | 31.0 ± 2.06 a | 210.75 ± 0.98 b |
| | 75 | 36.8 ± 0.36 bc | 30.1 ± 1.07 ab | 193.28 ± 2.05 bc |
| | 100 | 39.1 ± 0.43 b | 28.3 ± 0.95 b | 187.91 ± 1.98 c |
| 450 | 50 | 30.0 ± 3.95 d | 31.4 ± 5.05 a | 312.32 ± 3.75 a |
| | 75 | 33.9 ± 2.36 c | 28.6 ± 0.58 b | 300.39 ± 4.95 a |
| | 100 | 34.2 ± 1.25 cd | 27.2 ± 0.93 c | 283.64 ± 2.87 ab |

**The data were presented using the mean ± standard deviation (SD), and significant differences (P<0.05) at a 5% significance level were denoted by distinct lowercase letters next to the means.*

***PH, electric conductivity (EC), and cation exchange capacity (CEC)***

The pH values of biochar ranged from 7.55 to 8.40, and there was a non-significant increase (p>0) in pH with the increase in pyrolysis temperature and down feeding rate, as shown in Fig.4[A]. *Wu et al.* (*2012*) reported a similar finding. PH values of biochar produced from bamboo were around 8.2, according to *Abrishamkesh et al*. (*2015*), which is comparable to the biochar generated from rice husk. After pyrolysis, pH values change to a more alkaline value and may be applied to acidic soils for agricultural purposes like paddy cultivation (*Shen et al., 2014*). The results of this investigation show that the pyrolysis temperature greatly impacts the pH of rice husk biochar more than the feeding rate. *Wu et al.* (*2012*) and *Southavong et al.* (*2018*) also reached an identical conclusion. Nevertheless, studies of bamboo and rice husk biochar production showed that feeding rate had impacts on the physiochemistry, morphology, and spectroscopy of the biochar comparable to those of temperature (*Peng et al., 2011; Cantrell et al., 2012*).

EC increased with the biochar pyrolysis temperature. The EC was 0.206, 0.304, and 0.402 ds/m for 350, 400, and 450°C at 100 kg/h and increased to 0.253, 0.338, and 0.457 at 50 kg/h, respectively (Fig. 4[B]). When the temperature rose and the feed rate decreased, the ash content also increased, matching the rising trend in EC. Components previously dispersed throughout the ash content became concentrated there due to the loss of volatiles (*Cantrell et al., 2012*). This is because the K+ ion is more mobile in biochar, with a higher percentage of mineral ash probably having a greater electrical conductivity (*Joseph et al., 2007*).

Variance analysis also indicated no significant changes (p > 0.05) between the feeding rate of RH. In addition, the results illustrated in Fig. 4[C] present the CEC of biochar significantly reduced as the pyrolysis temperature increased (p < 0.05). CEC was 31.47, 26.70, and 22.71 cmol/kg for 350, 400, and 450°C at 50 kg/h and 32.45, 28.16, and 24.50 cmol/kg at 100 kg/h, respectively, which is consistent with *Graber et al.* (*2017*), *Huff et al.* (*2018*), and *Domingues et al.* (*2020*). When the temperature of the pyrolysis process rises, the aromatic carbon oxidation and the production of carboxyl groups in biochar contribute to a drop in the CEC (*Graber et al., 2017*). The prevalent phenolic, quinone, hydroxyl, and carbonyl groups also affect the CEC of biochar. The FTIR spectra (Fig. 3) reveal that free –OH bonds declined with increasing pyrolysis temperatures. *McBeath and Smernik* (*2009*) stated that the aromatization of carbon might have lowered the CEC in the ash of biochar created at high temperatures of 450°C.

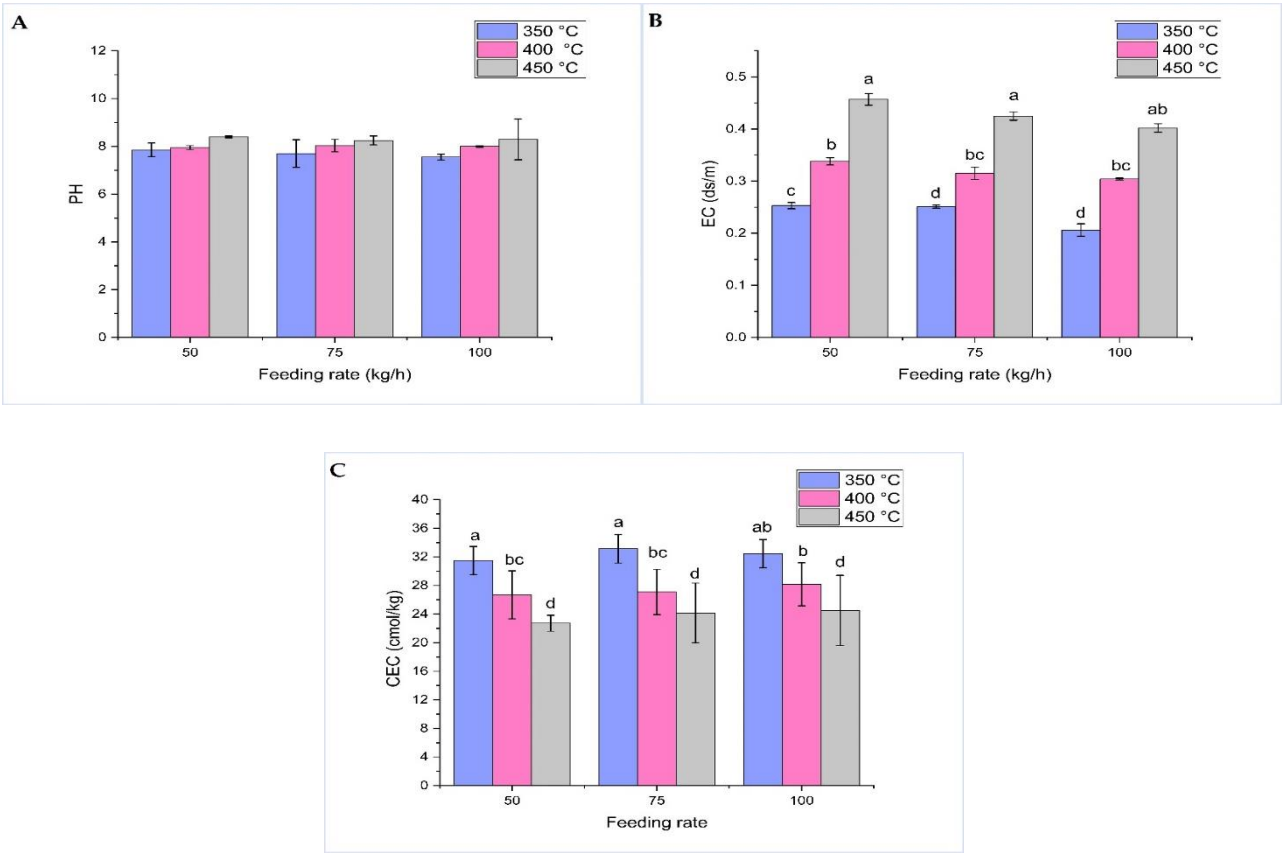


**Fig. 4 – Influence of the pyrolysis temperatures (350, 400, and 450°C) and feeding rate (50, 75, and 100 kg/h) on pH [A], EC [B], and CEC [C]**

## CONCLUSIONS

The biochar yield from rice husk biomass decreased as pyrolysis temperature increased but slightly increased as the feed rate increased. The maximum value of biochar ash content was obtained at a pyrolysis temperature of 450°C and a feeding rate of 50 kg/h. The BET surface area of the produced biochar mainly increased with increasing pyrolysis temperature, while the feeding rate was slightly affected. Both H and O values of the produced biochar increased with pyrolysis temperature and decreased with increased feeding rate. In contrast, an inverse pattern was observed for C and N values. The EC increased with the increase in pyrolysis temperature and decreased with the increase in feeding rate, while the CEC values showed an opposite trend. In general, biochar produced from rice husk (RH) at a pyrolysis temperature of 450°C and a feeding rate of 50 kg/h exhibited favorable chemical and physical features appropriate for enhancing soil quality.

## ACKNOWLEDGEMENT

The authors are most grateful to the Academy of Scientific Research and Technology (ASRT), Egypt, for funding the "Recycling of Agricultural Waste for Various Economic Products" project with ID No: 4539. The authors express their gratitude to the staff of the Agricultural Engineering Research Institute (AEnRI), Agricultural Research Center (ARC), Giza, Egypt, for their assistance with technical matters.

## REFERENCES

[1] Abrishamkesh, S., Gorji, M., Asadi, H., Bagheri-Marandi, G.H., & Pourbabaee, A.A. (2015). Effects of rice husk biochar application on the properties of alkaline soil and lentil growth. *Plant Soil Environ. 61*(11), 475–482. http://dx.doi.org/10.17221/117/2015-PSE

[2] Ahmad, M., Lee, S.S., Dou, X., Mohan, D., Sung, J-K., Yang, J.E., & Ok, Y.S. (2012). Effects of pyrolysis temperature on soybean stover-and peanut shell-derived biochar properties and TCE adsorption in water. *Bioresour. Technol*. *118*, 536–544. https://doi.org/10.1016/j.biortech.2012.05.042

[3] Alahakoon, A., Karunarathna, A.K., Dharmakeerthi, R.S., & Silva, F. (2022). Design and Development of a Double-chamber Down Draft (DcDD) Pyrolyzer for Biochar Production from Rice Husk. *J. Biosyst. Eng. 47*, 458–467. http://dx.doi.org/10.1007/s42853-022-00159-5

[4] Antal, M.J., & Grønli, M. (2003). The art, science, and technology of charcoal production. *Ind. Eng. Chem. Res. 42*(8), 1619–1640. http://dx.doi.org/10.1021/ie0207919

[5] Armynah, B., Djafar, Z., Piarah, W.H., & Tahir, D. (2018). Analysis of chemical and physical properties of biochar from rice husk biomass. *J. Phys. Conf. Ser. 979*, 12038. http://dx.doi.org/10.1088/1742-6596/979/1/012038

[6] Bray, R.H., & Kurtz, L.T. (1945). Determination of total, organic, and available forms of phosphorus in soils. *Soil Sci. 59*(1), 39–45. http://dx.doi.org/10.1097/00010694-194501000-00006

[7] Cantrell, K.B., Hunt, P.G., Uchimiya, M., Novak, J.M., Ro, & K.S. (2012). Impact of pyrolysis temperature and manure source on physicochemical characteristics of biochar. *Bioresour. Technol. 107*, 419–428. http://dx.doi.org/10.1016/j.biortech.2011.11.084

[8] Cao, X., & Harris, W. (2010). Properties of dairy-manure-derived biochar pertinent to its potential use in remediation. *Bioresour. Technol. 101*(14), 5222–5228. https://doi.org/10.1016/j.biortech.2010.02.052

[9] Chen, Y., Yang, H., Wang, X., Zhang, S., & Chen, H. (2012). Biomass-based pyrolytic polygeneration system on cotton stalk pyrolysis: influence of temperature. *Bioresour. Technol. 107*, 411–418. https://doi.org/10.1016/j.biortech.2011.10.074

[10] Claoston, N., Samsuri, A.W., Ahmad Husni, M.H., & Mohd Amran, M.S. (2014). Effects of pyrolysis temperature on the physicochemical properties of empty fruit bunch and rice husk biochars. *Waste Manag. Res. 32*(4), 331–339. https://doi.org/10.1177/0734242x14525822

[11] Demirbas, A. (2004). Effects of temperature and particle size on bio-char yield from pyrolysis of agricultural residues. *J. Anal. Appl. Pyrolysis 72*(2), 243–248. http://dx.doi.org/10.1016/j.jaap.2004.07.003

[12] Demirbas, A., Pehlivan, E., & Altun, T. (2006). Potential evolution of Turkish agricultural residues as bio-gas, bio-char and bio-oil sources. *Int. J. Hydrogen Energy 31*(5), 613–620. http://dx.doi.org/10.1016/j.ijhydene.2005.06.003

[13] Ding, Y., Liu, Y., Liu, S., Li, Z., Tan, X., Huang, X., Zeng, G., Zhou, L., & Zheng, B. (2016). Biochar to improve soil fertility. A review. *Agron. Sustain. Dev. 36*, 1–18. http://dx.doi.org/10.1007/s13593-016-0372-z

[14] Domingues, R.R., Sánchez-Monedero, M.A., Spokas, K.A., Melo, L.C.A., Trugilho, P.F., Valenciano, M.N., & Silva, C.A. (2020). Enhancing cation exchange capacity of weathered soils using biochar: Feedstock, pyrolysis conditions and addition rate. *Agronomy 10*(6), 824. https://doi.org/10.3390/agronomy10060824

[15] Dunnigan, L., Ashman, P.J., Zhang, X., & Kwong, C.W. (2018). Production of biochar from rice husk: Particulate emissions from the combustion of raw pyrolysis volatiles. *J. Clean Prod. 172*, 1639–1645. http://dx.doi.org/10.1016/j.jclepro.2016.11.107

[16] El-Sheikha, A.M., & Hegazy, R.A. (2020). Designing and Evaluating Biochar Pyrolysis Kiln. *J. Soil Sci. Agric. Eng. 11*(12), 701–707. https://dx.doi.org/10.21608/jssae.2020.159761

[17] Graber, E.R., Singh, B., Hanley, K., & Lehmann, J. (2017). Determination of cation exchange capacity in biochar. Biochar A Guid to Anal methods. Australia CSIRO. 74–84.

[18] Guo, J., & Lua, A.C. (1998). Characterization of chars pyrolyzed from oil palm stones for the preparation of activated carbons. *J. Anal. Appl. Pyrolysis 46*(2), 113–125.

[19] Gwenzi, W., Chaukura, N., Mukome, F.N.D., Machado, S., & Nyamasoka, B. (2015). Biochar production and applications in sub-Saharan Africa: Opportunities, constraints, risks and uncertainties. *J. Environ. Manage. 150*, 250–261. https://doi.org/10.1016/j.jenvman.2014.11.027

[20] Huff, M.D., Marshall, S., Saeed, H.A., Lee, & J.W. (2018). Surface oxygenation of biochar through ozonization for dramatically enhancing cation exchange capacity. *Bioresour. Bioprocess. 5*, 1–9. http://dx.doi.org/10.1186/s40643-018-0205-9

[21] Ibrahim, H.A-H. (2020). Introductory chapter: pyrolysis. Recent Adv Pyrolysis. London, United Kingdom: IntechOpen. http://dx.doi.org/10.5772/intechopen.90366

[22] Joardder, M.U.H., Halder, P.K., Rahim, M.A., & Masud, M.H. (2017). Solar pyrolysis: converting waste into asset using solar energy. *Clean Energy Sustain. Dev.* 213–235. https://doi.org/10.1016/B978-0-12-805423-9.00008-9

[23] Joseph, S.D., Downie, A., Munroe, P., Crosky, A., & Lehmann, J. (2007). Biochar for carbon sequestration, reduction of greenhouse gas emissions and enhancement of soil fertility; a review of the materials science. *Proc. Aust. Combust. Symp.* 130–133.

[24] Keiluweit, M., Nico, P.S., Johnson, M.G., & Kleber, M. (2010). Dynamic molecular structure of plant biomass-derived black carbon (biochar). *Environ. Sci. Technol. 44*(4), 1247–1253. https://doi.org/10.1021/es9031419

[25] Lehmann, J., & Joseph, S. (2015). Biochar for environmental management: an introduction. *Biochar Environ. Manag. Routledge*, 1–13.

[26] Lehmann, J., & Rondon, M. (2006). Bio-char soil management on highly weathered soils in the humid tropics, Biol approaches to Sustain soil Syst. CRC Press Boca Raton, FL;113, e530. http://dx.doi.org/10.1201/9781420017113.ch36

[27] Li, F., Cao, X., Zhao, L., Yang, F., Wang, J., & Wang, S. (2013). Short-term effects of raw rice straw and its derived biochar on greenhouse gas emission in five typical soils in China. *Soil Sci. Plant Nutr. 59*(5), 800–811. http://dx.doi.org/10.1080/00380768.2013.821391

[28] Liu, W-J., Jiang, H., & Yu, H-Q. (2015). Development of biochar-based functional materials: toward a sustainable platform carbon material. *Chem. Rev. 115*(22), 12251–12285. https://doi.org/10.1021/acs.chemrev.5b00195

[29] Lone, A.H., Najar, G.R., Ganie, M.A., Sofi, J.A., & Ali, T. (2015). Biochar for Sustainable Soil Health: A Review of Prospects and Concerns. *Pedosphere 25*(5), 639–653. http://dx.doi.org/10.1016/S1002-0160(15)30045-X

[30] Lynch, J., & Joseph, S. (2010). Guidelines for the development and testing of pyrolysis plants to produce biochar. Int. Biochar Initiat London, UK.

[31] Ma, Z., Chen, D., Gu, J., Bao, B., & Zhang, Q. (2015). Determination of pyrolysis characteristics and kinetics of palm kernel shell using TGA–FTIR and model-free integral methods. *Energy Convers. Manag. 89*, 251–259. http://dx.doi.org/10.1016/j.enconman.2014.09.074

[32] McBeath, A.V., & Smernik, R.J. (2009). Variation in the degree of aromatic condensation of chars. *Org. Geochem. 40*(12), 1161–1168. https://doi.org/10.1016/j.orggeochem.2009.09.006

[33] McElligott, K.M., Page-Dumroese, D.S., Coleman, M., & McElligott, K. (2011). Bioenergy production systems and biochar application in forests: Potential for renewable energy, soil enhancement, and carbon sequestration, US Department of Agriculture, Forest Service, Rocky Mountain Research. https://doi.org/10.2737/RMRS-RN-46

[34] Mukherjee, A., & Lal, R. (2014). The biochar dilemma. *Soil Res. 52*(3), 217–230. http://dx.doi.org/10.1071/SR13359

[35] Nan, H., Yin, J., Yang, F., Luo, Y., Zhao, L., & Cao, X. (2021). Pyrolysis temperature-dependent carbon retention and stability of biochar with participation of calcium: Implications to carbon sequestration. *Environ. Pollut. 287*, 117566. https://doi.org/10.1016/j.envpol.2021.117566

[36] Peng, X., Ye, L.L., Wang, C.H., Zhou, H., & Sun, B. (2011). Temperature-and duration-dependent rice straw-derived biochar: Characteristics and its effects on soil properties of an Ultisol in southern China. *Soil Tillage Res. 112*(2), 159–166. http://dx.doi.org/10.1016/j.still.2011.01.002

[37] Qu, J., Wang, Y., Tian, X., Jiang, Z., Deng, F., Tao, Y., Jiang, Q., Wang, L., & Zhang, Y. (2021). KOH-activated porous biochar with high specific surface area for adsorptive removal of chromium (VI) and naphthalene from water: Affecting factors, mechanisms and reusability exploration. *J. Hazard Mater. 401*, 123292. https://doi.org/10.1016/j.jhazmat.2020.123292

[38] Ren, D., Zhang, L., Huang, W., Cheng, H., He, T., & Meng, J. (2022). Design and test of key components of biochar return machine based on rocky. *INMATEH - Agricultural Engineering, 68*(3), 607–616. https://doi.org/10.35633/inmateh-68-60

[39] Ren, H., Guo, H., Shafiqul Islam, M., Zaki, H.E.M., Wang, Z., Wang, H., Qi, X., Guo, J., Sun, L., Wang, Q., Li, B., Li, G., & Radwan, K. (2023). Improvement effect of biochar on soil microbial community structure and metabolites of decline disease bayberry. *Front. Microbiol. 14*, 1154886. https://doi.org/10.3389/fmicb.2023.1154886

[40] Samsuri, A.W., Sadegh-Zadeh, F., & Seh-Bardan, B.J. (2014). Characterization of biochars produced from oil palm and rice husks and their adsorption capacities for heavy metals. *Int. J. Environ. Sci. Technol. 11*, 967–976. http://dx.doi.org/10.1007/s13762-013-0291-3

[41] Savova, D., Apak, E., Ekinci, E., Yardim, F., Petrov, N., Budinova, T., Razvigorova, M., & Minkova, V. (2001). Biomass conversion to carbon adsorbents and gas. *Biomass and Bioenergy 21*(2), 133–142. https://doi.org/10.1016/S0961-9534(01)00027-7

[42] Scholz, S.B., Sembres, T., Roberts, K., Whitman, T., Wilson, K., & Lehmann, J. (2014). Biochar systems for smallholders in developing countries: leveraging current knowledge and exploring future potential for climate-smart agriculture, World Bank Publications. http://hdl.handle.net/10986/18781

[43] Shen, J., Tang, H., Liu, J., Wang, C., Li, Y., Ge, T., Jones, D.L., & Wu, J. (2014). Contrasting effects of straw and straw-derived biochar amendments on greenhouse gas emissions within double rice cropping systems. *Agric. Ecosyst. Environ. 188*, 264–274. http://dx.doi.org/10.1016/j.agee.2014.03.002

[44] Song, W., & Guo, M. (2012). Quality variations of poultry litter biochar generated at different pyrolysis temperatures. *J. Anal. Appl. Pyrolysis 94*, 138–145. http://dx.doi.org/10.1016/j.jaap.2011.11.018

[45] Southavong, S., Ismail, M.R., Preston, T.R., Saud, H.M., & Ismail, R. (2018). Effects of pyrolysis temperature and residence time on rice straw-derived biochar for soil application. *Int. J. Plant Soil Sci. 23*(3), 1–11. http://dx.doi.org/10.9734/IJPSS/2018/42197

[46] Sun, X., Atiyeh, H.K., Li, M., & Chen, Y. (2020). Biochar facilitated bioprocessing and biorefinery for productions of biofuel and chemicals: A review. *Bioresour. Technol. 295*, 122252. https://doi.org/10.1016/j.biortech.2019.122252

[47] Tomczyk, A., Sokołowska, Z., & Boguta, P. (2020). Biochar physicochemical properties: pyrolysis temperature and feedstock kind effects. *Rev. Environ. Sci. BioTechnol. 19*, 191–215. https://link.springer.com/article/10.1007/s11157-020-09523-3

[48] Wu, W., Yang, M., Feng, Q., McGrouther, K., Wang, H., Lu, H., & Chen, Y. (2012). Chemical characterization of rice straw-derived biochar for soil amendment. *Biomass and Bioenergy 47*, 268–276. http://dx.doi.org/10.1016/j.biombioe.2012.09.034